INSTITUTE OF PHYSICS PUBLISHING JOURNAL OF PHYSICS: CONDENSED MATTER

J. Phys.: Condens. Matter **15** (2003) 3445–3470 PII: S0953-8984(03)60426-1

Oxidation state of uranium in metamict and annealed zircon: near-infrared spectroscopic quantitative analysis

Ming Zhang[1], **Ekhard K H Salje**[1] **and Rodney C Ewing**[2]

[1] Department of Earth Sciences, University of Cambridge, Downing Street, Cambridge CB2 3EQ, UK
[2] Department of Nuclear Engineering and Radiological Sciences, Department of Geological Sciences, University of Michigan, Ann Arbor, MI 48109-2104, USA

E-mail: mz10001@esc.cam.ac.uk

Received 6 March 2003
Published 12 May 2003
Online at stacks.iop.org/JPhysCM/15/3445

Abstract

Radiation and thermally induced changes in the oxidation state of uranium in metamict zircon have been systematically analysed, for the first time, using polarized near-infrared spectroscopy. The results showed that in damaged zircon U ions in crystalline domains exhibited relatively sharp, anisotropic signals from tetravalent and pentavalent U ions in crystalline domains ($U^{4+}_{crystal}$ and $U^{5+}_{crystal}$). The linewidths and peak positions of the 4834 cm^{-1} band ($U^{4+}_{crystal}$, $\boldsymbol{E} \parallel \boldsymbol{c}$) and the 6668 cm^{-1} band ($U^{5+}_{crystal}$, $\boldsymbol{E} \perp \boldsymbol{c}$) are a non-linear function of the self-radiation dose. They reach nearly constant values at doses greater than $\sim 3.5 \times 10^{18}$ α-events g^{-1}. Quantitative analysis of $U^{4+}_{crystal}$ and $U^{5+}_{crystal}$ signals revealed that the intensity ratio ($U^{4+}_{crystal}/U^{5+}_{crystal}$) exhibited a nearly linear increase as a function of dose and decreased on heating. This suggests that radiation leads to an alteration of the oxidation states of U and the tetravalent state is more preferable in radiation-damaged zircons. U ions associated with amorphous materials ($U_{amorphous}$) gave rise to broad and isotropic signals and they were mainly in the tetravalent state ($U^{4+}_{amorphous}$), although small amounts of pentavalent U ions ($U^{5+}_{amorphous}$) may exist. The dose dependence of the intensity ratio of $U_{amorphous}/U_{total}$ did not follow that of the reported fraction of the amorphous domain, but gave clearly lower values. This implies the potential preferential occurrence of U ions or possible U enrichment in the crystalline regions. Annealing intermediately and highly damaged zircon had different impacts on the oxidation state of U. An intermediately damaged zircon (with a dose of $\sim 5.2 \times 10^{18}$ α-events g^{-1}), annealed at high temperatures between 500 and 1800 K, showed a systematic increase in the signals of $U^{4+}_{crystal}$ and $U^{5+}_{crystal}$ above 700 K while $U^{4+}_{crystal}$ bands disappeared at temperatures above 1600 K. In contrast, a highly damaged zircon

(with a dose of $\sim 15.9 \times 10^{18}$ α-events g^{-1}) exhibited the presence of $U^{4+}_{crystal}$ and $U^{5+}_{crystal}$ above 1000 K, with a dramatic increase in signals near 1400 K.

1. Introduction

Zircon ($ZrSiO_4$; $I4_1/amd$) has a structure that is built of chains of alternating SiO_4 tetrahedra and ZrO_8 triangular dodecahedra parallel to the *c* axis (Speer 1980). U and Th are commonly found in natural zircon at concentrations that typically are no greater than 5000 ppm. Many zircon crystals are partially metamict (an aperiodic or amorphous state; Ewing 1994, Weber *et al* 1988, Salje *et al* 1999) as a result of self-radiation damage associated with the α-decay events of the incorporated U, Th and their daughter products.

Prior to this study there have been only limited studies of the effect of radiation damage on the oxidation state of uranium (Ellsworth 1925, Tomkeleff 1946, Hutton 1950, Frondel 1958). To gain an understanding of the oxidation state of U, which may occur in the tetra-, penta- and hexa-valent states, is of importance because the crystal chemistry and mobility of U varies with oxidation state, and these processes can have a profound effect on the results of U/Pb dating. In addition, as pointed out in our recent study (Zhang *et al* 2002), U ion absorption spectra are very sensitive to local symmetry; thus, by monitoring the spectral variations of U ions, one obtains an insight into local coordination environments as a function of increasing α-decay dose. Chemical analyses by electron microprobe, mass spectroscopy and ion microprobe (e.g. recent studies by Chapman and Roddick 1994, Davis and Krogh 2000, Carrigan *et al* 2002, Geisler *et al* 2002) have been used to study U concentrations in zircon, particularly the loss of U by diffusion and its effect on age determination. The bulk chemical analysis provides almost no structural or oxidation state information on uranium.

Although vibrational spectroscopy is sensitive to vibrational movements of molecules and atoms in crystals, the typical concentrations of U in natural zircon (e.g. thousands of parts per million) are not high enough to cause significant changes in vibrational spectra (in the frequency region below 1500 cm^{-1}). However, spectra related to the electronic state of U ions can be obtained in the near-infrared (NIR) region. In natural zircon, U atoms replace Zr atoms and occupy the Zr^{4+} site. The Zr^{4+} site is noncentrosymmetric, D_{2d}. Thus electronic transitions for paramagnetic impurities (e.g. U ions) are possible. Anderson and Payne (1939) and Anderson (1962, 1963) reported characteristic optical absorption spectra of U ions in natural zircon. Experimental and theoretical work has been performed to gain an understanding of the energy levels of U ions; U^{4+} and U^{5+} spectra of U-doped synthetic and heated natural zircon have been obtained (Judd and Runciman 1976, Kisliuk *et al* 1967, Richman *et al* 1967, Mackey *et al* 1975, Vance and Mackey 1974, 1975, 1978). The U energy levels can be labelled in terms of five irreducible representations of the D_{2d} point group: four singlets Γ_1, Γ_2, Γ_3, Γ_4 and one doublet Γ_5. The degenerate $5f^2(SL)J$ terms split into 70 levels: $16\Gamma_1 + 9\Gamma_2 + 12\Gamma_3 + 12\Gamma_4 + 21\Gamma_5$, i.e. 49 singlets Γ_1, Γ_2, Γ_3, Γ_4 and 21 doublets Γ_5.

In a recent NIR study on metamictization and recrystallization of zircon (Zhang *et al* 2002), we investigated the impact of radiation on defects (e.g. U and OH ions) in natural zircon and showed the evolution of U^{4+} and U^{5+} spectra, as well as modification of the OH signals with increasing degree of damage. The results showed that zircon samples with intermediate degrees of damage exhibited characteristic features that are different from those of crystalline or heavily damaged zircon. The changes, 'seen' by phonons (with a correlation length of a few unit cells) and defects such as U and OH ions, were explained by a radiation-induced change of local symmetry or a modification of the local configuration and a change of the oxidation state of uranium.

As a continuation of this previous work (Zhang *et al* 2002), we report, in this paper, newly recorded data and further analysis of the U ion spectra. We have obtained quantitative information on the spectral profiles of U ions as a function of increasing damage and have extracted the different contributions related to U ions in aperiodic and crystalline domains. In this application of infrared spectroscopy to the study of radiation damage in zircon, we demonstrate that it is possible to separate the U signals related to recrystallized and amorphous regions and to obtain the ratio of the two types of signals as a function of the degree of radiation damage. To our knowledge, these results are the first of their kind. We have obtained a quantitative analysis of U ion signals for metamict zircon and, by our analysis, have extracted the distribution of the different oxidation states of U in crystalline and amorphous regions in metamict and recrystallized zircon.

2. Experimental methods

2.1. Samples

The samples used in this study were mainly gemstone zircons from Sri Lanka, previously investigated by a number of different analytical methods (e.g. x-ray diffraction, FT-Raman and micro-Raman spectroscopy, IR and micro-IR spectroscopy, electron microscopy, electron microprobe, nuclear magnetic resonance) (Ellsworth *et al* 1994, Farnan and Salje 2001, Murakami *et al* 1991, Ríos and Salje 1999, Ríos *et al* 2000, Salje *et al* 1999, Zhang and Salje 2001, 2003, Zhang *et al* 2000a, 2000b, 2000c, 2002). Detailed information on these samples can be found in these references. These samples were chosen because they are well-characterized crystals of gemstone quality, have low levels of chemical impurities and lack of growth zoning. More importantly, Sri Lankan zircons can be found which are either crystalline or metamict due to the wide range of U and Th concentrations found in these samples (Holland and Gottfried 1955). The crystals used in this study were further investigated using IR microscopy (beam sizes of 80–150 μm) and the results showed that the spectral variations from point to point were very small. Apart from these Sri Lankan crystals, gem-quality crystalline zircon crystals from other localities studied previously (crystal Mud Tank, from Australia, studied by Murakami *et al* 1991, and crystal Moroto, studied by Zhang *et al* 2000a, 2000b and Farnan and Salje 2001) as well as a gem crystal with unknown locality (originally labelled Vigene) were used for the low-temperature measurement. More detailed information on crystals Mud Tank and Moroto can be found in the references given above. Electron microprobe analysis showed that the crystal labelled Vigene consisted of SiO_2 33.39, ZrO_2 66.59, HfO_2 0.86, Y_2O_3 0.03, ThO_2 0.01, UO_2 0.01 wt%, and Fe, Ca and Al with concentrations below our detection level. Its lattice parameters ($a = 6.6053$ Å, $c = 5.9802$ Å and $V = 260.96$ Å^3) were determined by x-ray Guinier powder diffraction with Si as internal standard. This sample showed polarized IR reflection features in the mid-IR region, similar to those of a crystalline zircon as reported by Zhang *et al* (2000c) and its reflectivity at 850 cm^{-1} ($\boldsymbol{E} \perp \boldsymbol{c}$) is 0.97, a value close to that of undamaged zircon (Zhang and Salje 2001). FT-Raman analysis (with an instrumental resolution of 2 cm^{-1}) showed that its ν_3 Raman mode (B_{1g}, antisymmetric stretching) is located near $\sim$1007 cm^{-1} with a measured full width at half maximum (FWHM) of $\sim$4 cm^{-1}. The radiation dose was estimated to be less than 1.0×10^{18} α-events g^{-1} based on a comparison with published data (e.g. Holland and Gottfried (1955) and Murakami *et al* (1991)) for x-ray data, Zhang *et al* (2000b) for polarized IR data and Zhang *et al* (2000c) for Raman data). Natural zircon may be subjected to thermal annealing during geological periods, thus affecting the amount of radiation damage that is retained in the sample. In this study, the self-radiation dose (based on the age of the zircon and its U and Th contents) for the natural

zircon crystals has been used to characterize the amount of damage. At present this is the best parameter to use in determining the extent of damage and will allow us to assess the relative changes in the crystalline and metamict domains of the zircon crystals.

The crystallographic orientations of the crystals were determined from the external morphology or by using x-ray precession techniques and an optical polarizing microscope. It was impossible to orient samples with doses higher than $\sim 10 \times 10^{18}$ α-events g^{-1}, as there were no easily obtained Bragg reflections and these high-dose crystals all had irregular external shapes. Crystal zircon plates were cut parallel to the *c* axis and then polished. Thermally treated samples were prepared by annealing the sample between 500 and 1800 K in air in a vertical furnace. The annealing temperature was measured with a Pt–PtRh thermocouple that was placed just above the samples. The zircon was annealed at a high temperature for 1 h and then quenched in air. After measurements at room temperature, the samples were annealed at a higher temperature.

3. Infrared technique

Infrared spectra were recorded using two IR spectrometers. A Bruker FT-IR 66v spectrometer attached to an infrared microscope was used to record the infrared spectra between 500 and 13 000 cm^{-1} at room temperature. A liquid-nitrogen-cooled MCT detector, coupled with a KBr beamsplitter and a Globar source, were used to record the spectra between 500 and 5000 cm^{-1}. For the frequency region of 3000–11 000 cm^{-1}, a tungsten source, an MCT detector and a CaF_2 beamsplitter were used with spectral resolutions of 2 and 4 cm^{-1}. A KRS5 wire-grid polarizer was employed. All the spectra were averaged over 512 scans. A Bruker 113v IFS spectrometer was used to record polarized and unpolarized infrared spectra between 4000 and 8000 cm^{-1} at low temperatures. An instrumental resolution of 1 cm^{-1} and 350 scans were adopted. A Leybold two-stage closed-cycle helium cryostat with a working temperature range of 13–310 K was used for the low-temperature measurements (Zhang *et al* 1996). The cryostat was coupled with a Leybold TLC60 temperature controller and a Leybold cryo-compresser. A sample holder was made from high-thermal-conductivity oxygen-free copper. A gold-coated lattice made from oxygen-free copper was installed at the sample position to improve the thermal contact between the sample and the sample holder. One temperature sensor, positioned near the heating unit, was used to control the temperature of the cryostat while another Si-diode temperature sensor (LakeShore, DT-470-DI-13, calibrated by the manufacturer) was glued onto the centre of the sample holder for measuring the sample temperature. The sample was placed in a vacuum chamber equipped with KRS5 windows. Sample and reference single-beam spectra measured at the same temperatures and in the same polarization conditions were used for calculating the absorption spectra. All absorption spectra were recorded as absorbance α, with $\alpha = -\log_{10}(I_{\text{sample}}/I_{\text{reference}})$, where I is the single-beam transmission intensity. The software OPUS-IR was used for data analysis. In order to obtain peak positions and FWHMs, the measured data were fitted to the Lorentzian functions with linear baselines.

4. Analysis and results

4.1. Radiation-induced spectral changes

Polarized U ion spectra (between 4000 and 11 000 cm^{-1}) of crystalline and metamict zircon are shown in figure 1(a). For crystalline zircon, our data are consistent with published results (Richman *et al* 1967, Vance and Mackey 1978), although some bands are too weak to be resolved at room temperature. We recorded absorption bands at 4838 and 10 922 cm^{-1} in

weakly damaged samples and they were assigned to $U^{4+}_{crystal}$ (Richman *et al* 1967, Vance and Mackey 1978). We use the subscript 'crystal' to indicate that the signal is associated with crystalline $ZrSiO_4$. The sharp bands near 6668 and 9030 cm^{-1} ($\boldsymbol{E} \perp \boldsymbol{c}$) are assigned as signals due to $U^{5+}_{crystal}$ in optical and Zeeman studies (Vance and Mackey 1974, 1975). Judd and Runciman (1976) proposed that they were due to $\Gamma_6 \rightarrow \Gamma_6$ and $\Gamma_7 \rightarrow \Gamma_7$ transitions. Experimental results (Vance and Mackey 1978) confirmed their prediction and revealed that there was no accidental degeneracy in the ground state of U ions. These authors found that it was caused by impurity-induced new transitions. In a recent classical atomic simulation study of zircon using the energy minimization approach, Akhtar and Waseem (2001) calculated defect energies to predict the most favourable site for an impurity ion in the host lattice of zircon and found that pentavalent ions could exist in zircon by metal vacancy compensation or electron compensation mechanisms.

The impact of radiation on the U ion spectra is characterized by three types of change described below.

(1) Isotropic, broad features appear in metamict zircon and their intensity increases with increasing degree of damage. As shown in figure 1(b), a broad feature occurs in the polarized spectra ($\boldsymbol{E} \parallel \boldsymbol{c}$ and $\boldsymbol{E} \perp \boldsymbol{c}$) between 4000 and 5600 cm^{-1} in heavily damaged samples. This feature is assigned as $U^{4+}_{amorphous}$ (the subscript 'amorphous' indicates that the signal is associated with the radiation-induced amorphous, or aperiodic, domains of $ZrSiO_4$) absorption because they are absent in the crystalline sample and disappear when annealed at high temperatures. Although the $U^{4+}_{amorphous}$ signals were the dominant components in spectra of high-dose samples (dose greater than $\sim 8 \times 10^{18}$ α-events g^{-1}), a broad, isotropic feature also appeared near 6700 cm^{-1}, but with a very weak intensity. The presence of this signal indicates that a small number of U ions are in the pentavalent state ($U^{5+}_{amorphous}$) in metamict natural $ZrSiO_4$. In highly damaged zircons, the ratio between the $U^{4+}_{amorphous}$ and $U^{5+}_{amorphous}$ absorption areas (integrated between 4500 and 5600 cm^{-1} for the $U^{4+}_{amorphous}$ signal, and between 6200 and 7150 cm^{-1} for the $U^{5+}_{amorphous}$ signal) gave an averaged value of $\sim 10\%$.
(2) The characteristic bands of crystalline materials show a systematic broadening and frequency shift (figures 1(a) and 2).
(3) The $U^{5+}_{crystal}$ band near 6668 cm^{-1} shows a relatively strong response to radiation damage in comparison with $U^{4+}_{crystal}$ as it became almost unresolvable above 7.5×10^{18} α-events g^{-1}, while weak $U^{4+}_{crystal}$ signals (e.g. near 4830 cm^{-1}) are still preserved.

4.2. Quantitative analysis of U^{4+} and U^{5+} signals

Spectral subtractions were conducted to separate the signals associated with crystalline materials from those of amorphous phases. In this approach, the damaged zircon was treated as a two-phase system (although the effective medium approach (Zhang and Salje 2001) is usually a better method, the different U concentrations in zircons with different degrees of damage made the application difficult). The subtraction was completed between two polarized spectra with different orientations recorded from the same crystal. The idea is based on the fact that, for a damaged sample, the signals related to crystalline regions remain essentially anisotropic even for damaged samples, whereas, signals from amorphous domains are independent of crystallographic orientations (i.e. the amorphization process destroys the long-range order of the crystal structure). Radiation-induced loss of anisotropy by metamictization of zircon has been shown previously by different studies, e.g. refractive index (Holland and Gottfried

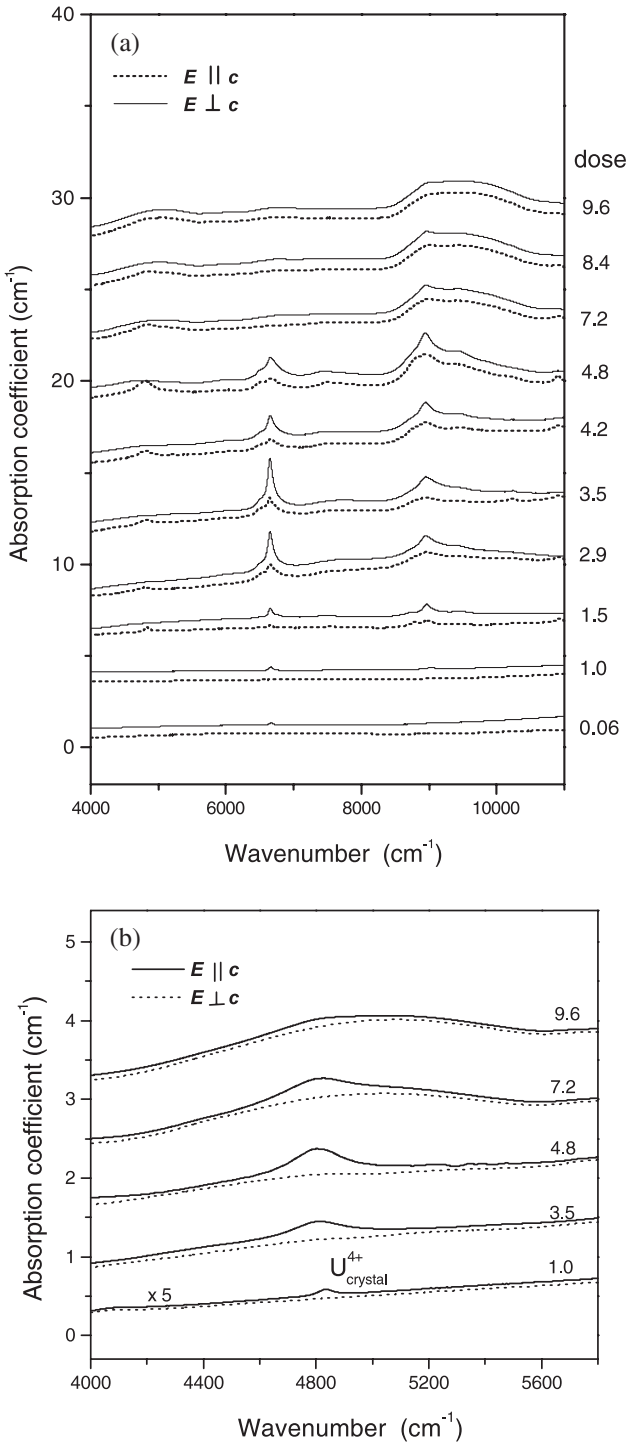

Figure 1. Polarized U ion spectra of metamict zircon (a) between 4000 and 11 000 cm^{-1} (the NIR data are from Zhang *et al* 2002). The indicated radiation dose represents the self-radiation dose of the natural zircon crystals accumulated since their growth. (b) Detailed feature between 4000 and 5800 cm^{-1}. The broad and isotropic U^{4+} feature in 4000–5600 cm^{-1} ($\boldsymbol{E} \perp \boldsymbol{c}$) was produced by metamictization.

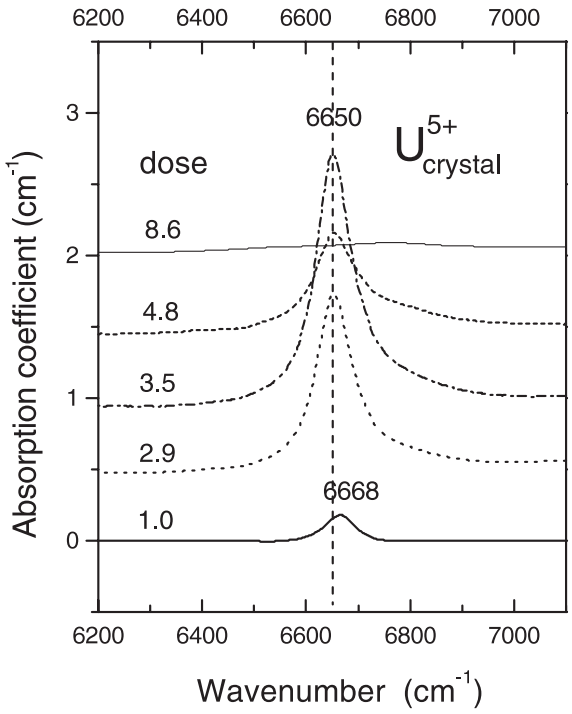

Figure 2. Difference spectra in the frequency region of 6200–7100 cm^{-1} ($A_{\boldsymbol{E}\perp\boldsymbol{c}} - A_{\boldsymbol{E}\parallel\boldsymbol{c}}$, where A represents absorption spectra).

1955), electron microscopy (Murakami *et al* 1991, Meldrum *et al* 1998), polarized infrared spectroscopy in mid-IR (Zhang *et al* 2000c), far-IR (Zhang and Salje 2001) and near-IR (Zhang *et al* 2002). Similar methods were successfully used to separate the OH signals associated with crystalline phases from those of amorphous domains in metamict titanite (Salje *et al* 2000, Zhang *et al* 2001). The advantage of using difference spectra from the same crystal is that this method can reduce the possible errors related to the measurements of different samples and also avoids the potential uncertainty caused by spectral variations associated with the amorphous zircon under further bombardments. To acquire better data for spectral subtraction and integration, particularly for high dose cases in which very limited crystalline regions remain, special measures were taken. Polarized reference single-beam spectra for both $\boldsymbol{E} \parallel \boldsymbol{c}$ and $\boldsymbol{E} \perp \boldsymbol{c}$ were recorded first in identical experimental conditions except rotating the polarizer remotely or manually; then, after sample loading, polarized sample single-beam spectra were recorded in the same experimental conditions as used in the reference spectrum measurements. These measures resulted in essentially consistent baselines and signal–noise ratios. In particular, this method ensured that the data measured with $\boldsymbol{E} \parallel \boldsymbol{c}$ and $\boldsymbol{E} \perp \boldsymbol{c}$ are from the same sample areas, with identical optical paths and sample thicknesses. These factors might affect the outcome of the subtractions and peak profile analysis (curve fit and integration). Typical difference spectra obtained through the spectrum subtraction are plotted in a stack in figures 2 and 3(a) (the inset part). The reasonable baselines and bandshapes suggest that the measurements and subtractions were well performed.

The 4834 cm^{-1} band ($U^{4+}_{crystal}$, $\boldsymbol{E} \parallel \boldsymbol{c}$) and the 6668 cm^{-1} band ($U^{5+}_{crystal}$, $\boldsymbol{E} \perp \boldsymbol{c}$) were used mainly for spectral analysis, as they are relatively intense and better separated from the

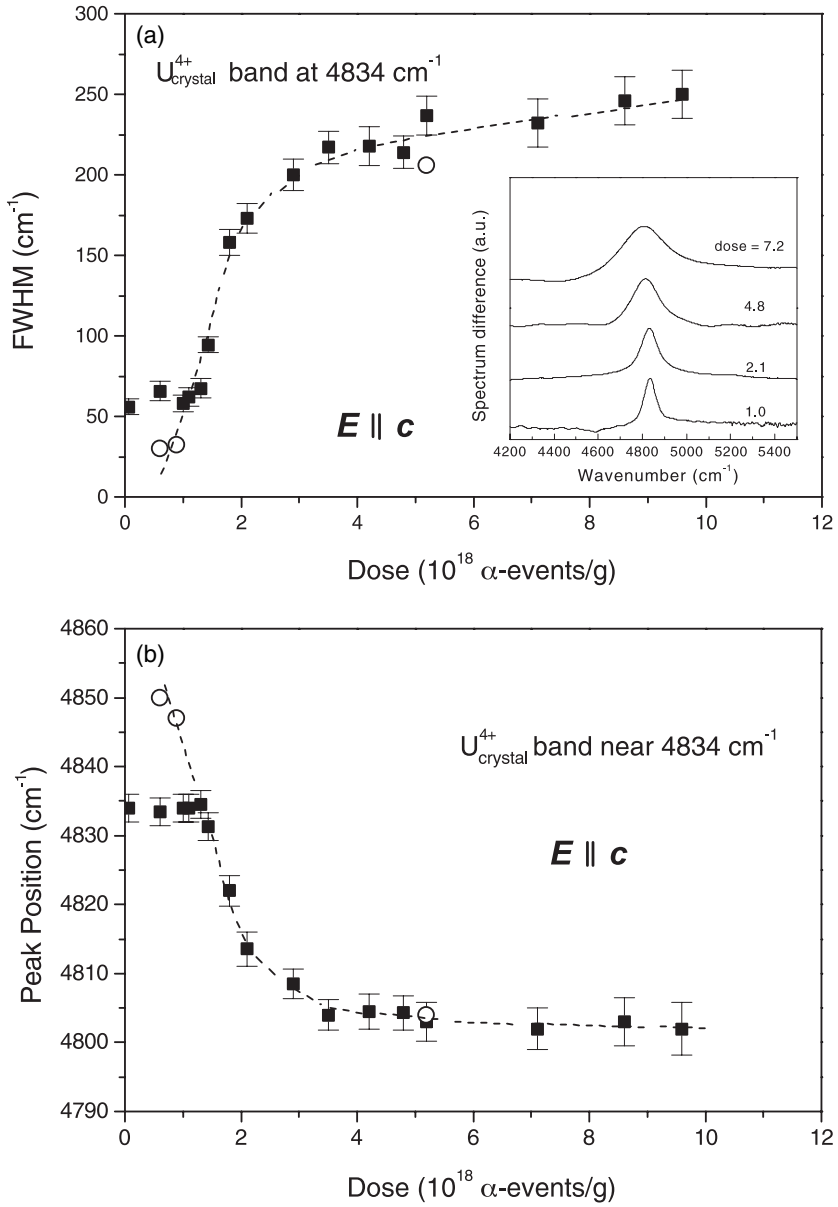

Figure 3. Dose dependence of peak positions and FWHM obtained from Sri Lanka zircon (full squares represent data obtained at room temperature, and open circles at 20 K): (a) FWHM of the 4834 cm^{-1} band ($U^{4+}_{crystal}$); (b) peak position of the 4834 cm^{-1} band; and (c) peak position of the $U^{5+}_{crystal}$ band near 6668 cm^{-1}. The inset in figure 3(a) shows the difference spectra between 4200 and 5500 cm^{-1} ($A_{E\|c} - A_{E\perp c}$,), which are normalized to show detailed changes of the band. The curves are visual guides.

other bands. Peak profile analysis was performed by fitting the $U^{4+}_{crystal}$ and $U^{5+}_{crystal}$ bands in the difference spectra to Lorentzian functions with linear baselines so as to gain quantitative results from the measured data. The FWHMs and peak positions of the $U^{4+}_{crystal}$ and $U^{5+}_{crystal}$

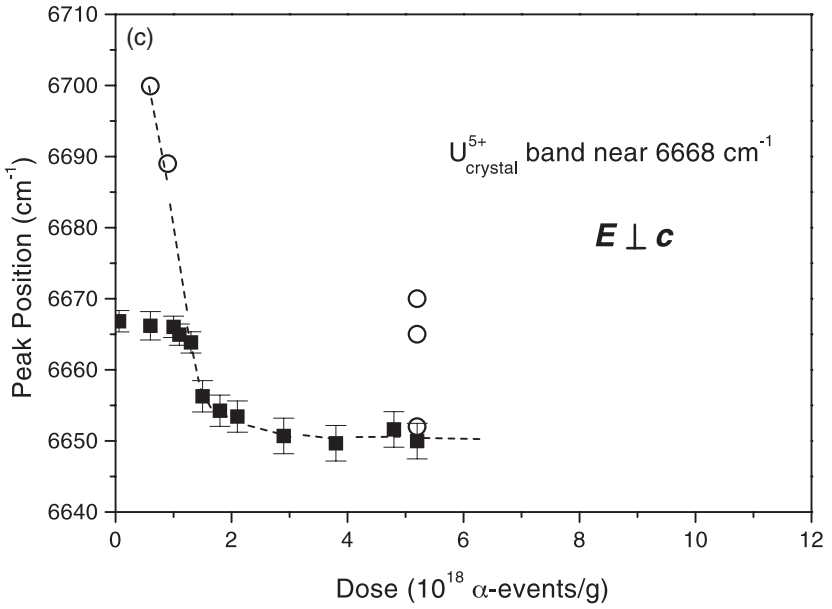

Figure 3. (Continued.)

are plotted as a function of radiation dose in figures 3(a)–(c). As the data were obtained from the difference spectra and the contributions of the amorphous domains were removed by spectral subtraction, the changes shown in figures 3(a)–(c) reflect mainly the behaviour of U ions in the crystalline regions. The peak profiles of the $U^{4+}_{crystal}$ near 4834 cm^{-1} shows a non-linear change with radiation dose (figure 3(a)). With increasing dose, its FWHM exhibits a dramatic increase in the dose region of ∼0 and ∼3.5 (10^{18} α-events g^{-1}), as shown in figure 3(a). It becomes almost saturated with further increasing dose. We consider that the dramatic frequency change and line-broadening in these U ion bands has the same physical nature as those frequency changes in Raman bands (e.g. the ν_3 mode near 1007 cm^{-1} as reported by Zhang *et al* (2000c)) that occur in the same dose region. They are associated with radiation-induced defective lattices. But the room-temperature data with doses of less than 1.0 (10^{18} α-events g^{-1}) (figures 3(a)–(c)) are of a more complex nature. We noted with surprise that, for crystalline zircon, the bands show FWHM values of 50–60 cm^{-1} at room temperature. This observation led us to suspect that these crystalline zircons could be more damaged than we had initially estimated. Our low-temperature results at 20 K (open circles) show that the plateau shown in figures 3(a) and (b) in this low-dose region is mainly caused by temperature-induced line broadening or frequency shift rather than, or weakly related to, radiation damage or structural disordering.

One of the important observations from this study is that in metamictization the $U^{5+}_{crystal}$ band near 6668 cm^{-1} ($\boldsymbol{E} \perp \boldsymbol{c}$) showed a much stronger decrease in intensity than that of the $U^{4+}_{crystal}$ band near 4834 cm^{-1} ($\boldsymbol{E} \parallel \boldsymbol{c}$) and the former became almost undetectable near a dose of 7.5 (10^{18} α-events g^{-1}) while for $U^{4+}_{crystal}$ the signal remained relatively intense. In order to compare the two types of signals quantitatively, the band areas of both signals were obtained by integrating the data shown in the difference spectra (figures 1(b) and 2). The ratio between these two band areas is plotted to reveal their relative change (figure 4(a)). The dose dependence of the ratio shows a systematic increase with increasing degree of damage. As the

data were extracted from the signals mainly related to crystalline regions, the results shown in figure 4(a) represent changes occurring in the remaining crystalline domains. We were unable to obtain data points at doses higher than ∼7.5 (10^{18} α-events g^{-1}), because the relatively sharp $U^{5+}_{crystal}$ signal becomes undetectable in the difference spectra (figure 2) as described earlier. With increasing radiation dose, the systematic change of the ratio between $U^{4+}_{crystal}$ and $U^{5+}_{crystal}$ ions implies radiation-induced variations of local charge state. We shall show in a later section that, during high-temperature annealing, the intensity ratio between $U^{4+}_{crystal}$ and $U^{5+}_{crystal}$ exhibits an opposite change: a systematic increase, indicating that the change shown in figure 4(a) is caused by radiation damage.

The ratio of the U ion signals contributed by those U ions in amorphous volumes ($U_{amorphous} = U^{4+}_{amorphous} + U^{5+}_{amorphous}$) and the total U ions ($U_{total} = U_{amorphous} + U^{4+}_{crystal} + U^{5+}_{crystal}$) was estimated (figure 4(b)). We found that it was very difficult or impossible to trace or integrate the $U^{5+}_{amorphous}$ component in zircon with intermediate degrees of damage, because of the low intensity of the component and the presence of weak sharp bands in the region, even for $\boldsymbol{E} \parallel \boldsymbol{c}$. In all our determinations of the $U^{5+}_{amorphous}$, the contribution of $U^{5+}_{amorphous}$ was considered as 10% of the $U^{4+}_{amorphous}$ (see above) value obtained from highly damaged samples (i.e. it was assumed that the ratio of $U^{4+}_{amorphous}$ to $U^{5+}_{amorphous}$ was a constant value in amorphous domains). This assumption is unlikely to result in any significant errors or influence our determination of the ratio, because the $U^{5+}_{amorphous}$ signal is very weak and plays a much less important role in the ratio.

4.3. U ion spectrum of decomposed zircon

To compare the spectral difference between metamict and decomposed zircon, we measured a decomposed zircon crystal from an unknown locality. The crystal (sample Cam1) was previously studied using Raman, x-ray and infrared (Zhang *et al* 2000c, 2002). The sample is a green gemstone, like most of the heavily damaged samples analysed. However, it shows Raman signals of $ZrSiO_4$ and additional sharp Raman bands at 146, 260, 312, 460 and 642 cm^{-1}, characteristic of tetragonal ZrO_2. X-ray diffraction data of Zhang *et al* (2000c) revealed that this zircon crystal is only partially metamict (with cell parameters $a = 6.6070$ Å, $c = 6.0221$ Å) and confirmed the presence of significant amounts of crystalline ZrO_2, consistent with infrared and Raman data. This decomposed zircon exhibits multi-phonon (overtone and combination) bands very different from the metamict zircon due to the presence of glassy SiO_2 (Zhang *et al* 2002). The U ion spectra of this crystal exhibit well-resolved spectral features and sharp U ions bands in contrast to other partially damaged samples (figure 5). The $U^{5+}_{crystal}$ signal near 6650 cm^{-1} is almost undetectable in this sample. Based on the high-temperature data, which shall be described in a later section, we consider that this decomposed sample was subjected to high temperature annealing.

4.4. Low-temperature spectra

Low-temperature measurements in the near-IR were completed with two objectives:

(1) to check whether radiation damage or structural disorder was responsible for the large room-temperature values (∼50–60 cm^{-1}) of the FWHMs recorded in crystalline samples (e.g. figure 3(a)), and
(2) to compare U ion spectra of crystalline and metamict zircon at low temperatures.

The low-temperature near-IR spectra from two samples with different degrees of damage are shown in figures 6(a) and (b) (with $\boldsymbol{E} \parallel \boldsymbol{c}$), and 6(c) and (d) (with $\boldsymbol{E} \perp \boldsymbol{c}$). Because U

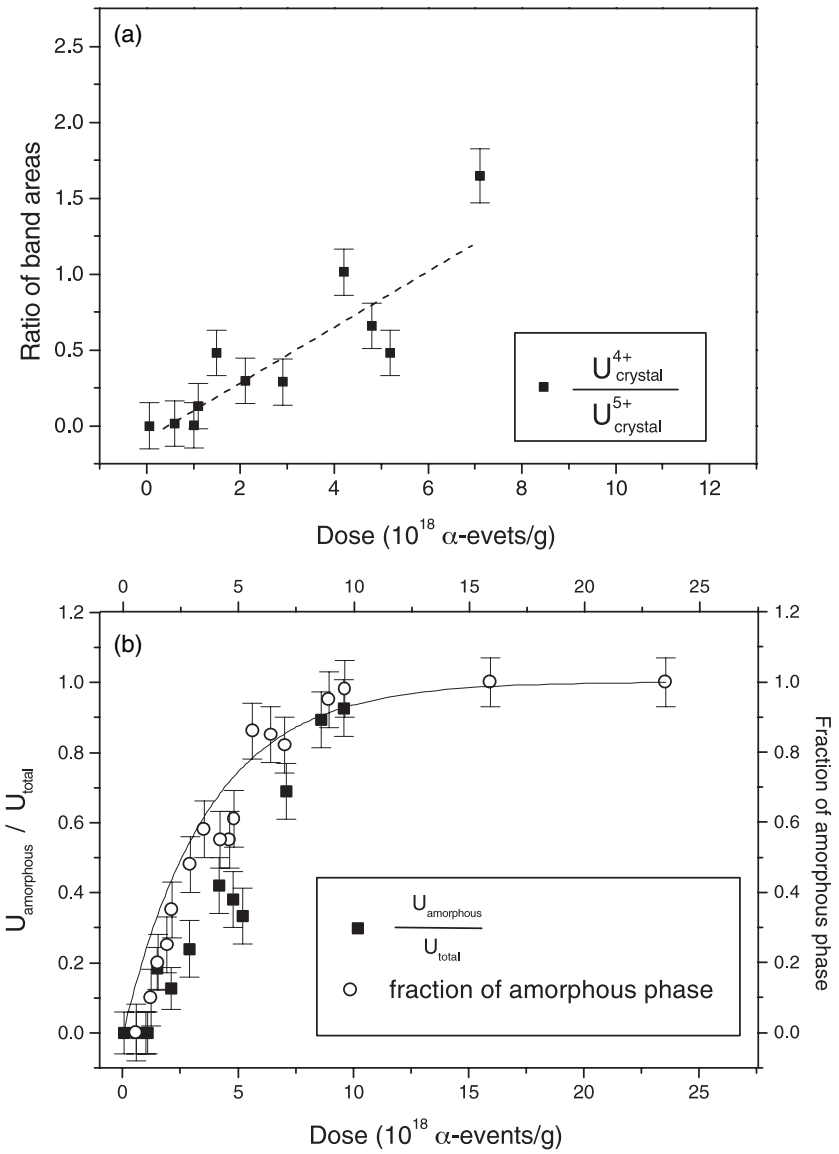

Figure 4. Dose dependence of the ratios of band areas (integrated absorption coefficients in units of cm^{-2}): (a) between the bands near 4834 cm^{-1} ($U^{4+}_{crystal}$) and near 6668 cm^{-1} ($U^{5+}_{crystal}$) (the data were obtained by integration of the bands in difference spectra; the line is a visual guide); (b) $U_{amorphous}/U_{total}$ (full squares) in comparison with the fraction of the amorphous materials (open circles—the IR data from Zhang and Salje 2001). The line is the function $f = 1 - e^{-B_a D}$ where D is radiation dose and $B_a = 2.7(3) \times 10^{-19}$ g is the amount of amorphous material produced per alpha-recoil (Ríos *et al* 2000).

concentrations in crystalline zircon are generally low ($UO_2 < 0.01$ wt% for our crystalline Sri Lanka zircon) and all our crystalline zircon crystals from Sri Lanka are very thin (100–200 μm in thickness), low-temperature U ion data from these Sri Lanka crystalline zircons did not give good signal-to-noise ratios in the polarized measurements. In addition, a relatively large crystal (sample Vigene with estimated dose of less than 1.0×10^{18} α-events g^{-1}

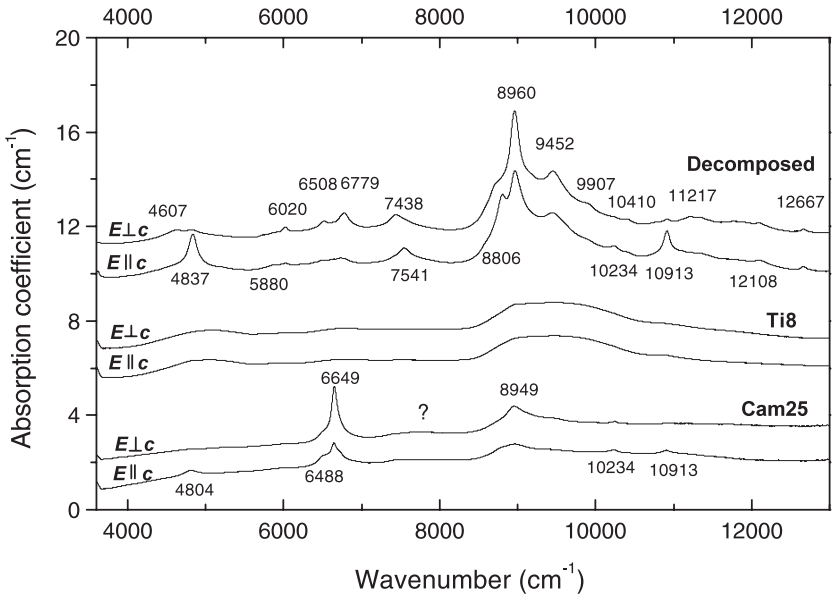

Figure 5. Comparison of U ion spectra of a decomposed zircon (Cam1), highly metamict zircon (Ti8) and a partially metamict zircon (Cam25).

and thickness of 4.7 mm) from an unknown locality was used. This sample shows two very weak bands ($\boldsymbol{E} \parallel \boldsymbol{c}$) located near 4072 and 4262 cm^{-1}, and both appear to have a similar intensity at room temperature. These two signals were not reported in previous studies and they could hardly be seen in our thin plates of Sri Lanka zircons. They might be due to the electronic transitions of U ions, because bands at 4032 and 4337 cm^{-1} were predicted by the calculation of Richman *et al* (1967), or they may be attributed to the combination of OH stretching and the vibrations of the framework.

The effect of cooling on U ion spectra is dramatic for this crystalline zircon (Vigene) (figures 6(b) and (d)). Although the sample shows a $U^{5+}_{crystal}$ band near 6668 cm^{-1} with a width of about 60 cm^{-1} at room temperature, the width decreases dramatically to 3.5 cm^{-1} at 20 K and the band shifts to 6700 cm^{-1}. The linewidth and frequency as a function of temperature were obtained by curve fitting (figures 7(a) and (b)). The linear correlation between the FWHM and temperature and the fact that it passes through the origin at 0 K indicates that for crystalline zircon large values of FWHMs at room temperature are simply caused by thermal vibration rather than the structural disordering. These results confirm that the crystalline samples used in this study are almost undamaged. However, in crystalline zircon crystals from Sri Lanka, Mud Tank and Moroto the U^{4+} band near 4834 cm^{-1} showed unexpected FWHMs of $\sim$30 cm^{-1} at 20 K.

In contrast to the crystalline zircon, decreasing temperature shows a much weaker effect on the U ion spectra of the partially damaged sample Cam25 ($\sim 5.2 \times 10^{18}$ α-events g^{-1}) (figures 6(a) and (c)). The $U^{5+}_{crystal}$ feature near 6651 cm^{-1} (the value at room temperature) of the sample becomes asymmetric at low temperatures. The bandshape seems to suggest that it consists of more than one band: one local maximum centred at 6670 cm^{-1} and the other two broad shoulders near 6665 and 6652 cm^{-1} (figures 3(c) and 6(c)). At 20 K the $U^{4+}_{crystal}$ band near 3802 cm^{-1} becomes sharper but its peak position is almost unchanged. The different temperature dependence of the near-IR signals between crystalline and metamict materials

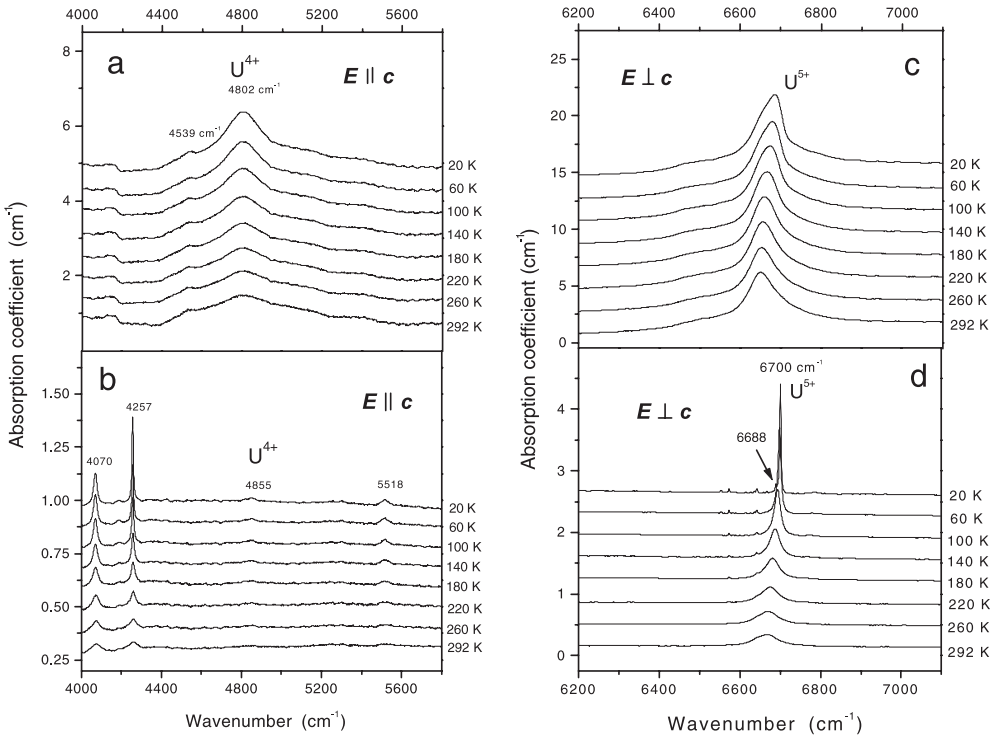

Figure 6. Polarized U ion spectra between 20 and 300 K. (a) Partially damaged zircon (Cam25, dose $= 5.2 \times 10^{18}$ α-events g^{-1}), 4000–5800 cm^{-1} ($\boldsymbol{E} \parallel \boldsymbol{c}$); (b) crystalline zircon (Vigene, estimated dose $< 1.0 \times 10^{18}$ α-events g^{-1}), 4000–5800 cm^{-1} ($\boldsymbol{E} \parallel \boldsymbol{c}$); (c) partially damaged zircon (Cam25), 6200–7100 cm^{-1} ($\boldsymbol{E} \perp \boldsymbol{c}$); (d) crystalline zircon (Vigene), 6200–7100 cm^{-1} ($\boldsymbol{E} \perp \boldsymbol{c}$).

is a result of radiation-induced structural variations between the crystalline and amorphous materials. Similar low-temperature behaviours were reported in OH species of crystalline and metamict zircons (Zhang *et al* 2002) and metamict titanites (Zhang *et al* 2000d).

For the crystalline sample shown in figure 6(b), a number of weak and sharp bands (near 6553, 6572, 6614, 6626, 6635, 6642, 6658, 6667 and 6689 cm^{-1}, with widths of 2–10 cm^{-1} at 20 K) were also detected at low temperatures. Changing temperature appears to have little impact on their frequencies. The physical nature of these weak bands is unclear. The possible causes include absorption bands by other rare-earth elements or new radiation-induced signals because some of them appear to be isotropic (they appear in both $\boldsymbol{E} \parallel \boldsymbol{c}$ and $\boldsymbol{E} \perp \boldsymbol{c}$ conditions with close intensities).

4.5. The effect of thermal annealing on U ion spectra

Metamict zircons were thermally annealed between 500 and 1800 K for 1 h in order to understand the response of U ions to heating and to investigate the different thermal effects on U ions for zircons with different degrees of damage. Annealed zircon crystals were quenched on the lab bench and measured at room temperature before heating to a higher temperature. Two Sri Lankan zircon crystals were used in the study. One was partially damaged (sample Cam25, $\sim 5.2 \times 10^{18}$ α-events g^{-1}) and the other is highly metamict (sample Sd4, $\sim 15.9 \times 10^{18}$ α-events g^{-1}). Our results show that the thermal behaviour of U ions depends

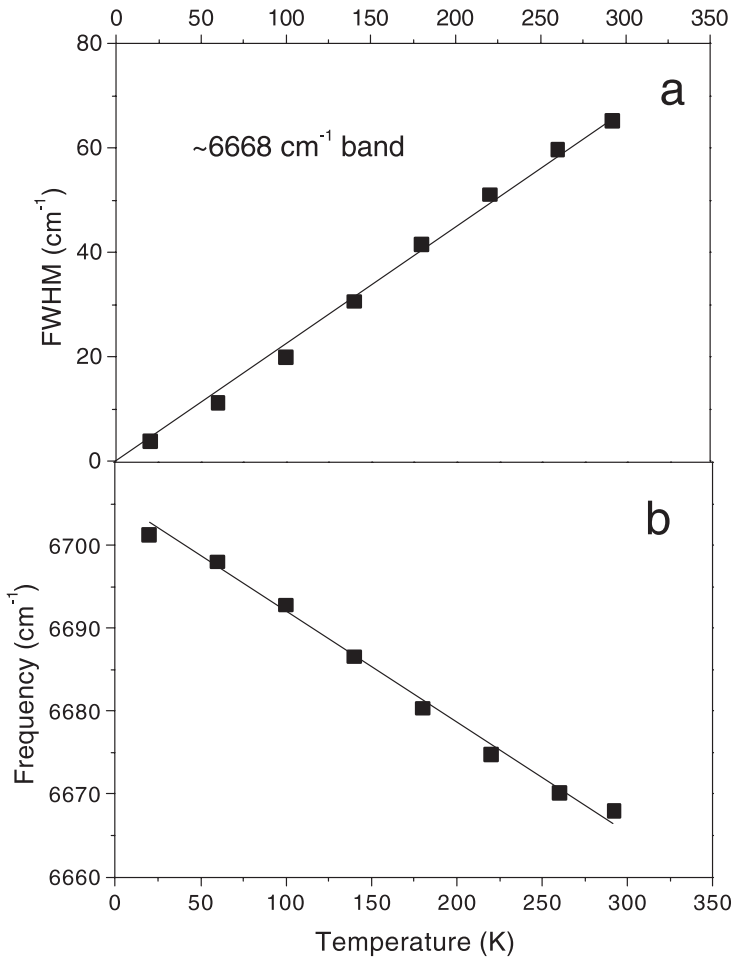

Figure 7. Temperature evolution of the peak profiles of the band near 6669 cm^{-1}: (a) FWHM, and (b) peak position. The lines are visual guides.

on the initial degree of damage of the samples. Thus, we shall describe the changes in partially and highly metamict zircon separately. As shown in figures 8(a)–(d), annealing a partially metamict sample (Cam25) at 500 K did not cause detectable spectral changes. Dramatic modifications of the spectra occurred near 1000 and 1600 K. We noted that $U^{4+}_{crystal}$ and $U^{5+}_{crystal}$ signals show the following different types of changes on heating:

(1) The signals characteristic of crystalline materials show an increase in intensity (integrated absorption) taking place near 600 K. However, the $U^{4+}_{crystal}$ signal near 4830 cm^{-1} did not show a significant increase in intensity until 800 K (figures 8(a) and 10(b)), although it exhibits band sharpening at temperatures above 700 K.
(2) A band near 9804 cm^{-1} ($\boldsymbol{E} \parallel \boldsymbol{c}$) becomes active between 1000 and 1100 K, and it shows an increase in intensity with further heating. The physical origin of this band is unclear.
(3) At temperatures between 1500 and 1600 K, the $U^{4+}_{crystal}$ bands at 4832, 8796 and 10 916 cm^{-1} ($\boldsymbol{E} \parallel \boldsymbol{c}$) disappeared (figure 8(a)), accompanied by a frequency shift of the 9018 cm^{-1} signal.

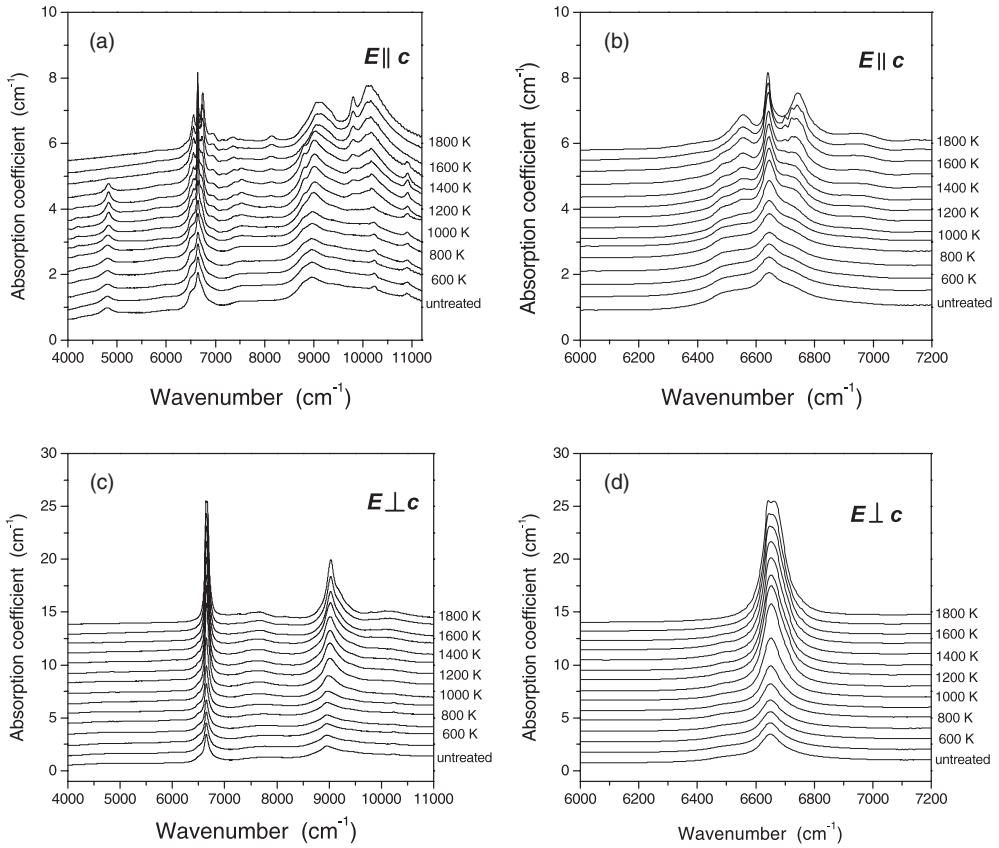

Figure 8. Polarized U ion spectra of a partially metamict zircon (Cam25) annealed between 500 and 1800 K. (a) Between 4000 and 11 000 cm^{-1} ($\boldsymbol{E} \parallel \boldsymbol{c}$); (b) detailed changes between 6000 and 7200 cm^{-1} ($\boldsymbol{E} \parallel \boldsymbol{c}$); (c) between 4000 and 11 000 cm^{-1} ($\boldsymbol{E} \perp \boldsymbol{c}$); and (d) detailed changes between 6000 and 7200 cm^{-1} ($\boldsymbol{E} \perp \boldsymbol{c}$).

We recorded a few unexpected weak and sharp absorption bands. They appeared near 6698, 6721, 6740 and 6759 cm^{-1} between 1500 and 1700 K. Above 1600 K, the $U^{5+}_{crystal}$ band near 6650 cm^{-1} ($\boldsymbol{E} \perp \boldsymbol{c}$) appears to become two local maxima (figure 8(c)). More detailed changes in the region of 6000 and 7200 cm^{-1} can be seen in figures 8(b) and (d). Peak profile analysis was performed for the $U^{4+}_{crystal}$ band near 4830 cm^{-1} and the $U^{4+}_{crystal}$ band near 6650 cm^{-1}. The FWHM and peak position of the $U^{4+}_{crystal}$ band are plotted as a function of temperature in figures 9(a) and (b). The data show that both spectral parameters begin to recover between 700 and 800 K. We note that the frequency (figure 9(b)) exhibits a change like that observed in Raman spectra of the ν_3 mode of SiO_4 tetrahedra (B_{1g}, antisymmetric stretching) (Zhang *et al* 2000c): a dramatic increase between 700 and 1100 K and temperature independence or weak dependence above ∼1100 K.

The integral absorption coefficient (in units of cm^{-2}) for the $U^{5+}_{crystal}$, $U^{4+}_{crystal}$ and $U_{amorphous}$ signals was obtained (figures 10(a)–(c)). It is interesting that the $U^{5+}_{crystal}$ signal near 6652 cm^{-1} shows an increase of ∼200% in intensity between 600 and 1200 K, while the $U^{4+}_{crystal}$ signal near 4830 cm^{-1} exhibits only ∼20% increase for the same temperature region, accompanied by an unexpected decrease in the intensity of signals from the amorphous domains beginning

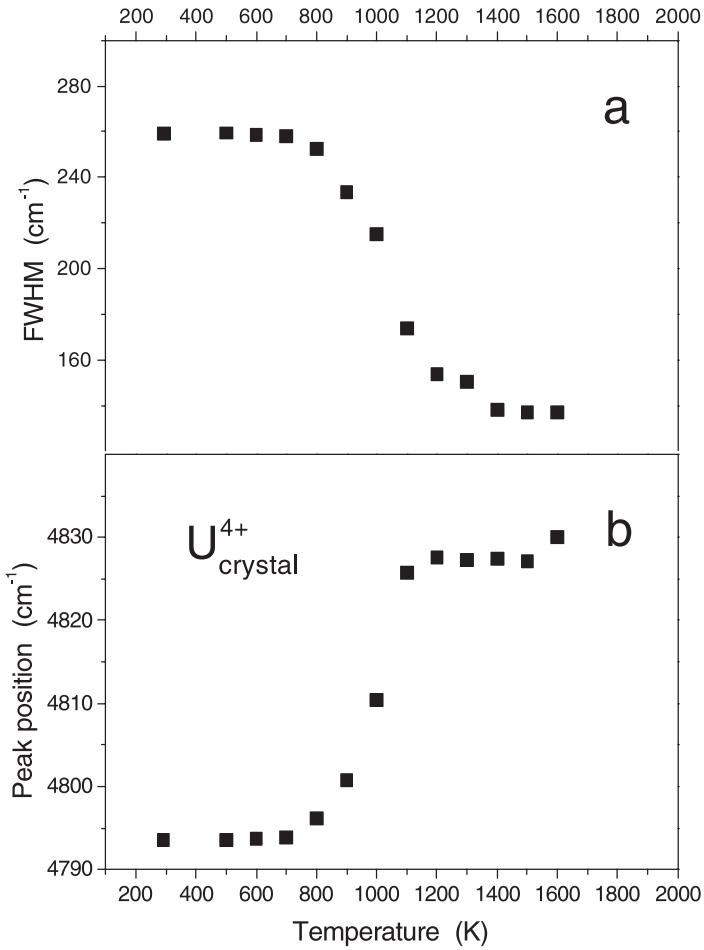

Figure 9. Temperature dependence of peak profiles of the U^{4+} band near 4832 cm^{-1} (sample Cam25). (a) FWHM and (b) peak position.

at ∼700 K. The decrease is likely caused by epitaxial growth of the remaining crystalline domains in this moderately damaged sample. Epitaxial growth in radiation-damaged zircon has been previously reported in the polarized IR reflection study of Zhang *et al* (2000b), who observed the recovery of anisotropy along the original crystallographic orientations in damaged zircon on heating and a systematic increase in the reflectivity of zircon starting near 700 K. Our results indicate a possible alteration of the charge state during thermal annealing. The ratios of band areas for $U^{4+}_{crystal}/U^{5+}_{crystal}$ and $U_{amorphous}/U_{total}$ were obtained and are shown as a function of annealing temperature in figures 11(a) and (b). The systematic changes in the intensity ratios on heating shown in figures 11(a) and (b) confirm that the changes shown in figures 4(a) and (b) are caused by radiation damage. The results show that the ratios of the different signals can be altered by thermal process.

The data of an annealed high-dose zircon crystal from Sri Lanka (Sd4, with a dose of 15.9×10^{18} α-events g^{-1}) measured by Zhang *et al* (2002) was analysed in order to compare the thermal behaviours of U ions in partially and highly metamict zircon. The crystal was annealed up to 1800 K in time steps of 1 h at different temperatures in a N_2 atmosphere

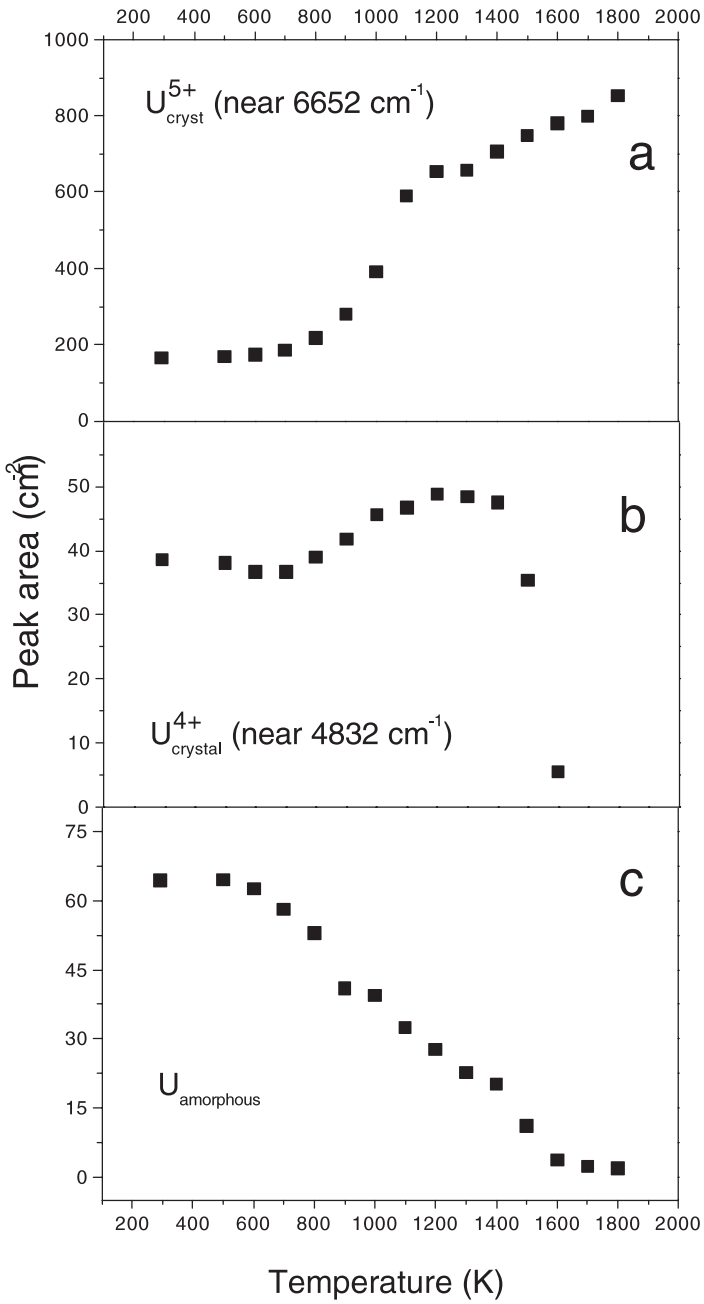

Figure 10. Temperature dependence of band areas (in units of cm^{-2}) (sample Cam25): (a) $U^{5+}_{crystal}$ near 6652 cm^{-1} ($\boldsymbol{E} \perp \boldsymbol{c}$); (b) $U^{4+}_{crystal}$ near 4832 ($\boldsymbol{E} \parallel \boldsymbol{c}$); and (c) signals due to U ions in the amorphous region. The data of $U_{amorphous}$ were obtained by integrating the absorption coefficient ($\boldsymbol{E} \perp \boldsymbol{c}$) between 4000 and 5600 cm^{-1} in figure 8(c).

(figure 12). Due to the reasons explained in the experimental section, it was impossible to orient this high-dose sample crystallographically, and only unpolarized spectra were recorded. The

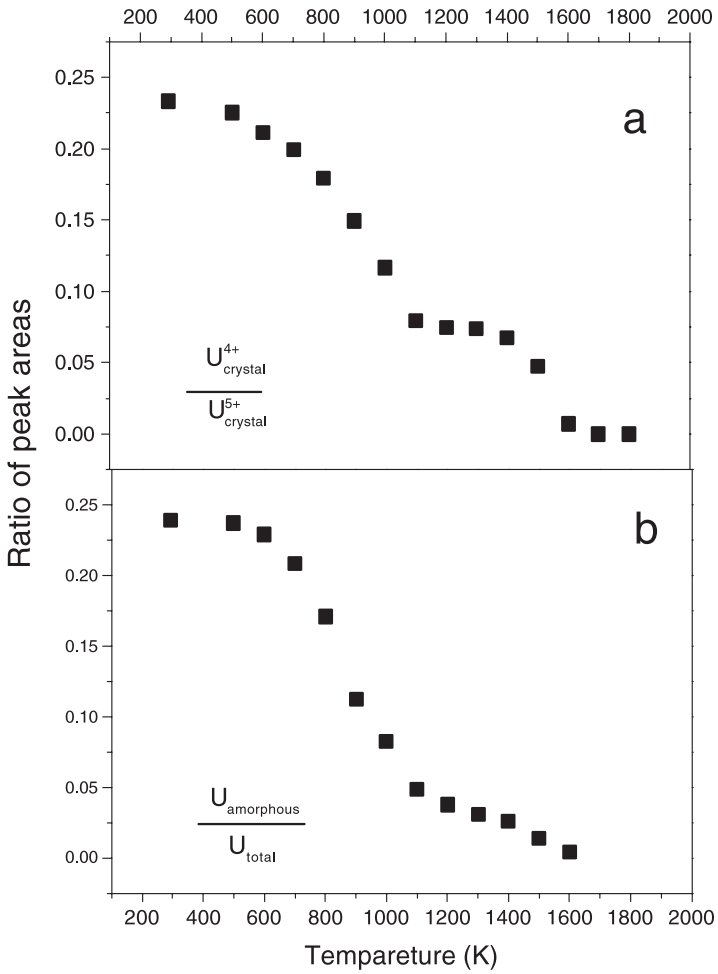

Figure 11. Ratio of band areas as a function of annealing temperature (sample Cam25): (a) $U^{4+}_{crystal}/U^{5+}_{crystal}$ and (b) $U_{amorphous}/U_{total}$.

structural recovery and recrystallization of the sample are characterized by infrared reflectance data on vibrations of SiO_4 groups (650–1400 cm^{-1}, room temperature–1800 K) and multi-phonon spectra (1400–2500 cm^{-1}) of the annealed sample (shown in the insets of figure 12). No significant spectral variations are detected at temperatures below 1000 K. As shown in the inset of figure 12, a broad shoulder near 1948 cm^{-1} appears near 1100 K. This feature becomes more visible in the 1200 K spectrum. This feature indicates the appearance of SiO_2 glass resulting from the partial decomposition of this heated high-dose zircon (Zhang *et al* 2002). The thermal-induced decomposition was confirmed by Raman spectrum of this sample annealed at 1100 and 1200 K, which shows the presence of tetragonal ZrO_2. After annealing at 1400 and 1500 K, the crystal shows the characteristic broad multi-phonon signals of crystalline $ZrSiO_4$ near 1515, 1592, 1595, 1836, 1871, 1903, 1950 and 1992 cm^{-1} (obtained using the secondary-derivative method) (the right inset in figure 12), indicating the significant crystal growth of $ZrSiO_4$. A sharpening of these curves and an increase in their intensity are observed with further increases in temperature.

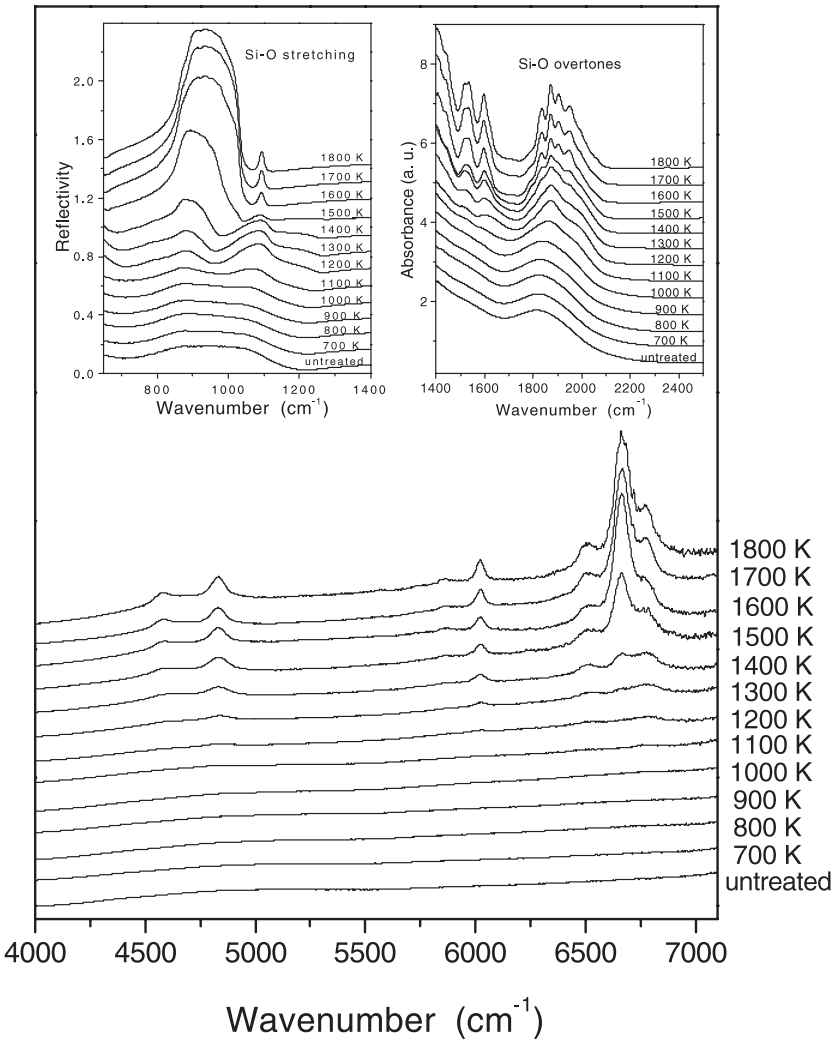

Figure 12. Unpolarized U ion spectra of a highly metamict zircon (sample Sd4, dose $=\sim 15.9 \times 10^{18}$ α-events g^{-1}) up to 1800 K (the data are from Zhang *et al* 2002). It was impossible to orient this high-dose sample crystallographically. The spectra were recorded using a Globar source, a KBr beamsplitter and a MCT detector.

Systematic changes in U spectra (figure 12) resulted from the recrystallization of this highly damaged zircon. In contrast to the thermal behaviour of the intermediately damaged zircon (Cam25), no significant spectral changes were recorded below ∼1000 K, i.e. the spectra of this highly damaged zircon were still dominated by broad features related to those in the amorphous domains at these temperatures. This implies that the thermal behaviour depends on the degree of initial damage in the sample. Weak and relatively sharp U ion signals became detectable between 1100 and 1300 K. Further heating resulted in a dramatic increase in the intensity of the signals, especially for $U^{5+}_{crystal}$ bands. The integrated absorbance of the 4830 cm^{-1} ($U^{4+}_{crystal}$) and the 6652 cm^{-1} ($U^{5+}_{crystal}$) signals was extracted through curve fitting to show the effect of annealing temperature (figure 13(a)). The dramatic increase of U ion signals that occurred near 1400 K (figure 12) is explained as an indication of the growth of $ZrSiO_4$ resulting from

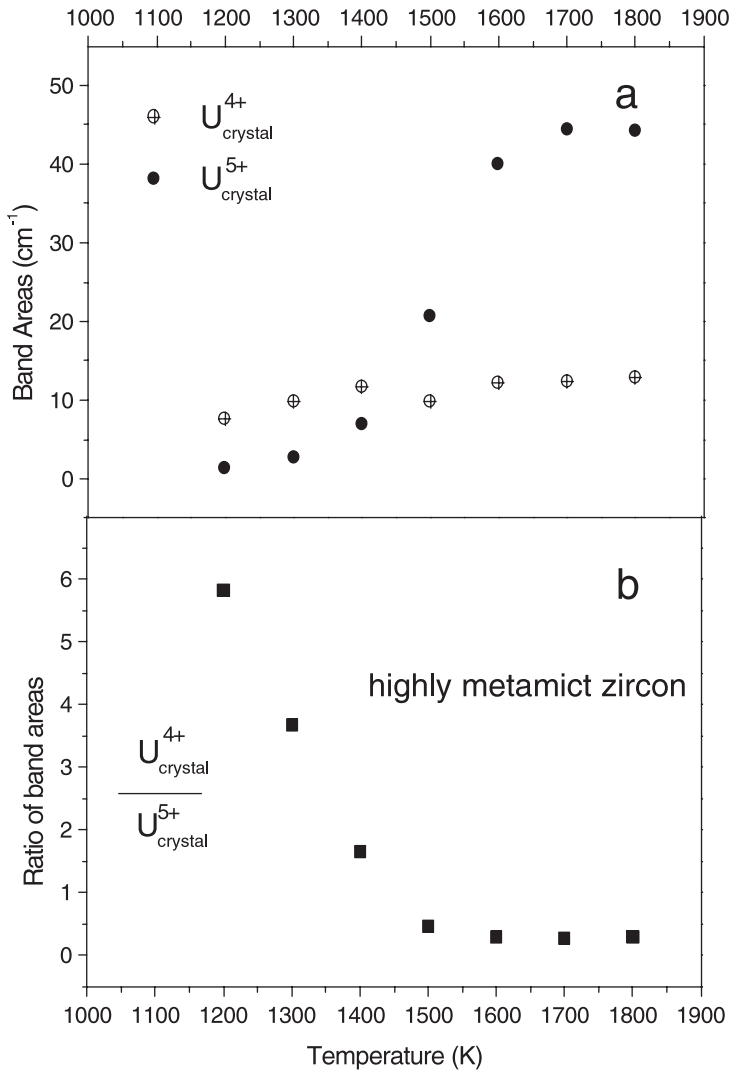

Figure 13. Temperature dependence of band areas and ratio of band areas of the highly damaged zircon Sd4. (a) Band areas of the $U^{5+}_{crystal}$ signal near 6652 cm^{-1} and the $U^{4+}_{crystal}$ signal near 4830 cm^{-1}; and (b) $U^{4+}_{crystal}/U^{5+}_{crystal}$.

the reaction of ZrO_2 and SiO_2 (Zhang *et al* 2002). Our data show that the oxidation state of uranium in metamict zircon can be dramatically altered in metamictization and thermal annealing.

5. Discussion

Our analysis demonstrates that the U ion signals of metamict zircon can be simplified into two types with different structural origins:

(1) lines from U ions ($U^{4+}_{crystal}$ and $U^{5+}_{crystal}$) in the remaining crystalline regions showing anisotropic and relative sharp bands, and

(2) absorption of U ions ($U_{amorphous}$, mainly in tetravalent state) from amorphous materials exhibiting broad and isotropic spectral features.

With changing radiation dose, the systematic change in intensity ratio between these two types of signals (figure 4(b)) is essentially associated with the change of the volumes of the two types of material (although, strictly, it does not represent the fraction of the amorphous materials), in contrast to the change between $U^{4+}_{crystal}$ and $U^{5+}_{crystal}$ caused by radiation-induced ionization. This result is supported by the opposite changes in the two types of signal during radiation damage and thermal annealing. We believe that in damaged zircon the U ions associated with the $U^{4+}_{crystal}$ and $U^{5+}_{crystal}$ signals occupy structural sites (U for Zr) in $ZrSiO_4$ and the local structure is defective and distorted by radiation. In unannealed zircons, a majority portion of these $U^{4+}_{crystal}$ and $U^{5+}_{crystal}$ ions could enter the Zr^{4+} sites when the crystal first forms (of course, $U^{5+}_{crystal}$ is charge compensated). The original ratio of $U^{4+}_{crystal}$ and $U^{5+}_{crystal}$ might depend on the growth conditions (e.g. temperature and pressure). This means that $U^{4+}_{crystal}$ and $U^{5+}_{crystal}$ are more likely associated with ^{238}U and ^{235}U ions in crystalline regions (if neglecting radiogenic U ions). Please note that our data shown in figure 4(b) suggest radiogenic U ions might also be present in crystalline regions (see later discussions).

The $U_{amorphous}$ ions in the glassy/amorphous materials, however, are formed through a different process. It is generally accepted that the recoils ($\sim$0.7 MeV) produced during α-decay events are mainly responsible for the formation of the amorphous domains in metamict zircon (Weber *et al* 1988). As the crystalline and amorphous states in zircon are very different structurally, these U ions in amorphous regions must have undergone structural rearrangements, and they are no longer associated with their original local configurations formed at the time of crystallization. Although there is a lack of knowledge of the local structure of the amorphous domains, it is clear that long and medium order of the crystal structure of zircon is destroyed or lost (Murakami *et al* 1991, Weber *et al* 1988, Salje *et al* 1999, Zhang and Salje 2001). At this stage, we can attribute the $U_{amorphous}$ to different types of U ions with different types of sources: radiogenic U ions through alpha decays (e.g. ^{234}U ions) and undecayed U ions (^{238}U and ^{235}U) that are in the way of the high-energy recoils or located within the recoil-impact areas. They are more likely to be affected by different processes (e.g. hydrothermal alteration, dissolution, and weathering) because of the amorphous structure. Recent experimental results (Davis and Krogh 2000) reported preferential dissolution of ^{234}U from radiation-damaged zircon. Leaching of U, Th and radiogenic daughters from monazite was documented by Eyal and Olander (1990) and Olander and Eyal (1990a, 1990b).

The results in figure 4(b) show that the dose dependence of the ratio of $U_{amorphous}/U_{total}$ does not follow that of the fraction of the amorphous domain, but gave clearly lower values. The apparent suggestion of the data is that a lower portion of U ions is found in the amorphous domains as compared to the fraction of amorphous material. If this is true, the direct implication from the results is the preferential occurrence of U ions or possible U enrichment in the crystalline regions. The physics behind the difference between the data of the fraction and the $U_{amorphous}/U_{total}$ appears complex. Based on the data, one may speculate whether some ^{234}U ions (e.g. produced in the decay of Th) appear in the crystalline region of the damaged zircon (or possibly end up in the Zr^{4+} sites) or some of the U ions in amorphous materials were somehow leached out during geological periods. The latter does not seem the case for the Sri Lanka zircon gem crystals used in this study because they showed very low OH or H_2O contents (Woodhead *et al* 1991a, 1991b, Zhang *et al* 2002) and the data from the mid-IR region (Zhang and Salje 2001) do not show characteristic spectral features seen recently in fluid-altered zircons produced through hydrothermal leach experiments (Geisler *et al* 2003). The understanding of the data in figure 4(b) is further complicated by other factors related to

the radiation damage in metamict zircon. For instance, the amorphous materials in metamict zircon are produced by the α-decay radiation of U, Th and their daughter products, but the data shown in figure 4(b) are mainly associated with U ions. The other issue one might need to take into account is whether the molar absorption coefficients of the different U ions remain constant even in the whole dose region (or whether radiation damage leads to changes of the molar absorption coefficients). These complex issues are beyond the scope of this study and more work is desirable.

We shall focus on the radiation-induced changes associated with the U ions in the crystalline materials (i.e. $U^{4+}_{crystal}$ and $U^{5+}_{crystal}$). One important issue related to the metamictization process in zircon is the nature behind some similarities between the results of U ion spectra and phonon spectra (e.g. Raman spectra) of zircon. As shown in figures 3(b) and (c), the frequencies of the U ion bands exhibited a systematic decrease in the dose region of $\sim$0 and $\sim$3.5 (10^{18} α-events g^{-1}). A similar change was reported in a Raman study on phonon modes of damaged zircons (Zhang *et al* 2000c). These authors showed that crystalline zircon exhibited a Raman band near 1007 cm^{-1} (internal ν_3 band of SiO_4) and its frequency lowered to $\sim$995 cm^{-1} with increasing dose up to $\sim$3.5 (10^{18} α-events g^{-1}) as a result of percolation of the amorphous phases (Salje *et al* 1999). On annealing, the frequency of the Raman band recovered (Zhang *et al* 2000a). As these two types of spectroscopic methods reveal information from different length scales (phonon spectra are associated with molecular/atomic vibrations, whereas U ion spectra are related to electronic transitions), the similar changes in both types of spectra probably reflect the same physical origin from different aspects, and it is impossible that these anomalies, detected by different analytic methods, could appear accidentally in the same dose region. The change in U ion spectra likely results from the radiation-induced defective structure of zircon revealed by x-ray diffraction and vibrational spectroscopy (Murakami *et al* 1991, Zhang *et al* 2000a, 2000c). The radiation-induced changes in the defective zircon lattice are shown in U spectra through the strong coupling between the electronic transitions within the f band and the vibrations of the host lattice in materials with zircon structure (Lahalle *et al* 1986). Another possible cause is the potential alteration of the averaged symmetry (D_{2d}) of a Zr^{4+} site in damaged zircon, as high concentrations of impurities can result in the breaking of the site symmetry. Unfortunately, there is a lack of experimental investigations into this issue because of its complexity.

With increasing metamictization, the increase in the signal ratio between tetravalent and pentavalent U ions in crystalline domains (figure 4(a)) and the observation of dominated U^{4+} signals in amorphous domains (figure 1(a)) indicate that the tetravalent state (i.e. with electronic charge of 4+) is the preferable oxidation state of U ions in metamict zircon. The increase in the ratio of $U^{4+}_{crystal}/U^{5+}_{crystal}$ can be explained as trapping electrons by the pentavalent U ions and changing to the tetravalent state. On heating the trapped electron could be released and leads to the decrease in the ratio of $U^{4+}_{crystal}/U^{5+}_{crystal}$ as shown in figures 11(a) and 13(b). In this case the electrons are expected to be deeply trapped, in contrast to those trapped by other defects (e.g. see below), as on heating the change in $U^{4+}_{crystal}/U^{5+}_{crystal}$ appeared above 700 K. The change could also be the result of a radiation-induced change of local structures, which could lead to modifications of the local configurations associated with Zr^{4+} and Si^{4+} sites.

The results of this study shed light on several aspects of the crystal chemistry of zircon and the issues could have significant implications in geology and mineralogy.

(1) As pointed out by Zhang *et al* (2002), ionization may occur during radioactive decay (i.e. α-, β- and γ-decays), causing variations of the charge state of lattice defects. To gain further understanding of radiation-induced changes in valence states of metamict materials is of importance as these changes may play a significant role in the microstructural

evolution of irradiated materials and result in changes in other physical properties (Ewing 2001). As a result, the mobility of the defects may be affected (Bourgoin and Corbett 1978) and eventually the chemical durability and dissolution rate may be altered. This may affect the leaching behaviour of natural zircon and the related diffusion processes. In addition, the modification of charge states can change the local configurations associated with hydrous components and give rise to new sites for OH species in zircon. Thus, element migration in metamict materials is a critical issue for candidate materials proposed for the immobilization and stabilization of nuclear waste forms. Our observations of radiation-induced ionization in metamict zircon draw our attention to several important questions, such as whether the ionization may possibly influence the diffusion and leach behaviour of trace elements, especially on U and Pb ions, in natural zircon, or whether the different types of U ion components (e.g. $U_{amorphous}$, $U^{4+}_{crystal}$, $U^{5+}_{crystal}$) exhibit different diffusion behaviour. It appears reasonable to think that $U_{amorphous}$ can be more easily leached out from metamict zircon, compared with $U^{4+}_{crystal}$ and $U^{5+}_{crystal}$, as damaged zircons generally show much high leach rates (Ewing *et al* 1982) and the U ions in amorphous materials should have weaker interactions with other atoms and poorly defined crystal fields. Based on the general concept of ions, we can predict that $U^{4+}_{crystal}$ and $U^{5+}_{crystal}$ should have different diffusion rates because of their different ionic radii. Ions with smaller ionic radius may show higher diffusion coefficients and better mobility, although we have no knowledge on whether there is a preferential loss between $U^{4+}_{crystal}$ and $U^{5+}_{crystal}$.

(2) Investigations into defects or impurities-related charge states may shed light on the nature of site occupancies and the forms of the relevant charge compensation occurring as a result of radiation damage. In general, when cations with different valence states appear in the zircon structure, oxygen vacancies or hole formations are required for charge compensation to neutralize the system. Radiation damage may lead to changes of crystal fields near the cation sites, migrations of different vacancies/holes and electron trapping with defects. Similar to the change of U ions in zircon, the alteration of the charge states for Dy and Tb ions ($Dy^{3+} \leftrightarrow Dy^{4+}$ and $Tb^{3+} \leftrightarrow Tb^{4+}$) was documented in irradiated and annealed zircon (Laruhin *et al* 2002). To gain a better understanding of the oxidation state of Pu in Pu-doped zircon and the potential alteration of the valence state is of considerable importance as zircon has been proposed as a waste form for the disposal of plutonium from dismantled nuclear weapons (Burakov 1993, Anderson *et al* 1993, Ewing *et al* 1995, Weber *et al* 1996, Ewing 1999). Plutonium may exist in different valence states (e.g. 3+, 4+, 5+ and 6+) (see, e.g., Conradson *et al* 1998). In Pu-doped zircon Pu sits in the Zr^{4+} site (with a symmetry of D_{2d}) through chemical substitutions. As oxidation or reduction can result in a significant variation in structural distortion due to the change in ionic size mismatch between cations with different charges on the Zr^{4+} sites, the structural parameters can be altered remarkably. For instance, data from crystalline ^{239}Pu-substituted zircon (Begg *et al* 2000) showed that annealing the crystalline sample at 1200 °C for 12 h in air led to the oxidation of Pu^{3+} (the trivalent state of Pu in the zircon was an unexpected result of originally preparing the Pu-substituted zircon under a reducing atmosphere) to Pu^{4+} and this resulted in the decrease of the cell volume from 267.8 to 262.3 Å^3. The relative large ionic radius of Pu^{3+} (the ionic radius of plutonium ions can be ∼0.100 and ∼0.086 Å for Pu^{3+} and Pu^{4+}, respectively (Shannon 1976, Williford *et al* 2000), in comparison to 0.79 Å for Zr^{4+} (Akhtar and Waseem 2001)) might also alter the preferred mechanism for incorporation of these ions into the zircon lattice. Computer simulation (Williford *et al* 2000) has shown that two Pu^{3+} ions can be charge compensated by an oxygen vacancy, although Pu^{4+} substitution of Zr^{4+} has the lowest energy. Investigations have shown that relatively low energy irradiation (e.g. γ-ray irradiation) can cause other defect centres in

zircon. The formation of SiO_m^{n-} defects in zircon were reported in different studies (Barker and Hutton 1973, Solntsev *et al* 1974, Laruhin *et al* 2002). During irradiation, some of the oxide ions in the zircon crystal structure lose an electron, which can be trapped by silicon oxide groups forming SiO_4^{5-}, SiO_2^{3-} and SiO_2^-. Some of the radicals were stabilized by a Zr vacancy or by some atom incorporated substitutionally for Zr in the lattice of $ZrSiO_4$. However, these defects are less stable upon heating compared to our case because these defects act as shallow electron/hole traps. EPR (electron paramagnetic resonance) data of irradiated zircons showed that these SiO_m^{n-} defect centres can be annealed at temperatures between 373 and 423 K (Laruhin *et al* 2002). The presence of these different defects in natural zircons and their disappearance at different temperatures on heating may provide a potential means to examine the thermal history of the host rocks.

(3) To gain better understanding of radiation-induced ionization is important for theoretical simulations in studies in petrology and mineralogy, as different trace REEs (rare-earth element) in natural zircon have been commonly used for modelling of petrogenetic process and metamorphism. One of the examples is the use of REEs to determine partition coefficients of zircon/melt and to study the composition of the melt from which the zircon host crystallized. Previous studies showed that zircon/melt partition coefficients strongly depend on cation radius and their values can vary over several orders when the cation radius changes from 0.97 to 1.15 Å (Watson 1980, Murali *et al* 1983, Fujimaki 1986, Thomas *et al* 2002). However, the different valence states of REEs in zircon were reported (e.g. Gaft *et al* 2000, Akhtar and Waseem 2001, Laruhin *et al* 2002) and they can potentially result in problems. For instance, in zircon, Ce ions are in the form of Ce^{4+} and Ce^{3+}. The commonly obtained partition coefficient for Ce represents an apparent coefficient that includes both Ce^{4+} and Ce^{3+}. However, the different ionic radii between Ce^{4+} and Ce^{3+}($Ce^{4+} = 0.97$ Å and $Ce^{3+} = 1.143$ Å) result in a considerable difference between the partition coefficients of Ce^{3+} and Ce^{4+} ($D_{Ce^{3+}} = 0.14$ and $D_{Ce^{4+}} = 102.6$) (Thomas *et al* 2002). Any potential change of the charge state between two types of ions caused by radiation over geological periods could alter the results of natural systems and consequently complicate data interpretation and theoretical modelling.

Acknowledgments

The authors would like to thank Steve Laurie at the Sedgwick Museum (University of Cambridge, UK), Andrew Clark and Mark Welch at the Natural History Museum (London, UK) and Jochen Schlüter at the Mineralogisches Museum (Universität Hamburg, Germany) for providing some of the samples used in this study. Thanks are due to William Lee for reading the original manuscript. Financial funding from British Nuclear Fuels (BNFL) and the Cambridge-MIT Institute (CMI) is gratefully acknowledged. RCE gratefully acknowledges financial support from the US Department of Energy, Office of Basic Energy Sciences (DE-FG02-97ER45656).

References

Akhtar M J and Waseem S 2001 *Chem. Phys.* **274** 109
Anderson B W 1962 *Gemmologist* **31** 19
Anderson B W 1963 *J. Gemmol.* **9** 1
Anderson B W and Payne C J 1939 *Gemmologist* **9** 1
Anderson E B, Burakov B E and Vasiliev V G 1993 *Proc. Safe Waste '93* **2** 29
Barker V P and Hutton D R 1973 *Phys. Status Solidi* b **60** K109
Begg B D, Hess N J, Weber W J, Conradson S D, Scheiger M J and Ewing R C 2000 *J. Nucl. Mater.* **278** 212

Bourgoin J C and Corbett J W 1978 *Radiation Effects* **36** 157
Burakov B E 1993 *Proc. Safe Waste '93* **2** 19
Carrigan C W, Miller C F, Fullagar P D, Bream B R, Hatcher R D Jr and Coath C D 2003 *Precambrian Res.* **120** 1
Chapman H J and Roddick J C 1994 *Earth Planet. Sci. Lett.* **121** 601
Conradson S D, Al Mahamid I, Clark D L, Hess N J, Hudson E A, Neu M P, Palmer P D, Runde W H and Tait C D 1998 *Polyhedron* **17** 599
Davis D W and Krogh T E 2000 *Chem. Geol.* **172** 41
Ellsworth H V 1925 *Am. J. Sci.* **209** 127
Ellsworth S, Navrotsky A and Ewing R C 1994 *Phys. Chem. Minerals* **21** 140
Ewing R C 1994 *Nucl. Instrum. Methods Phys. Res.* B **91** 22
Ewing R C 1999 *Proc. Natl Acad. Sci., USA* **96** 3432
Ewing R C 2001 *Can. Mineral.* **39** 697
Ewing R C, Haaker R F and Lutze W 1982 *Mater. Res. Soc. Symp. Proc.* **11** 389
Ewing R C, Lutze W and Weber W J 1995 *J. Mater. Res.* **10** 243
Eyal Y and Olander D R 1990 *Geochim. Cosmochim. Acta* **54** 1867
Farnan I and Salje E K H 2001 *J. Appl. Phys.* **89** 2084
Frondel C 1958 *US Geol. Surv. Bull.* **1064** 400
Fujimaki H 1986 *Contrib. Mineral. Petrol.* **94** 42
Gaft M, Panczer G, Reisfeld R and Shinno I 2000 *J. Alloys Compounds* **330/301** 267
Geisler T, Pidgeon R T, van Bronswijk W and Kurtz R 2002 *Chem. Geol.* **191** 141
Geisler T, Zhang M and Salje E K H 2003 *J. Nucl. Mater.* at press
Holland H D and Gottfried D 1955 *Acta Crystallogr.* **8** 291
Hutton C O 1950 *Bull. Geol. Soc. Am.* **61** 635
Judd B R and Runciman W A 1976 *Proc. R. Soc.* A **352** 91
Kisliuk P, Richman I and Wong E Y 1967 Absorption spectrum of U^{4+} in zircon ($ZrSiO_4$) *Optical Properties of Ions in Crystals* ed H M Crosswhite and H W Moos (New York: Wiley-Interscience) p 537
Lahalle M P, Krupa J C, Lepostollec M and Forgerit J P 1986 *J. Solid State Chem.* **64** 181
Laruhin M A, van Es H J, Bulka G R, Turkin A A, Vainshtein D I and den Hartog H W 2002 *J. Phys.: Condens. Matter* **14** 3813
Mackey D J, Runciman W A and Vance E R 1975 *Phys. Rev.* **155** 262
Meldrum A, Zinkle S J, Boatner L A and Ewing R C 1998 *Nature* **395** 56
Murali AV, Parthasarathy R, Mahadevan TM and Sankar D 1983 *Geochim. Cosmochim. Acta* **47** 2047
Murakami T, Chakoumakos B C, Ewing R C, Lumpkin G R and Weber W J 1991 *Am. Mineral.* **76** 1510
Olander D R and Eyal Y 1990a *Geochim. Cosmochim. Acta* **54** 1879
Olander D R and Eyal Y 1990b *Geochim. Cosmochim. Acta* **54** 1889
Richman I, Kisliuk P and Wong E Y 1967 *Phys. Rev.* **155** 262
Ríos S and Salje E K H 1999 *J. Phys.: Condens. Matter* **11** 8947
Ríos S, Salje E K H, Zhang M and Ewing R C 2000 *J. Phys.: Condens. Matter* **12** 2401
Salje E K H, Chrosch J and Ewing R C 1999 *Am. Mineral.* **84** 1107
Salje E K H, Zhang M and Groat L A 2000 *Phase Transit.* **71** 173
Shannon R D 1976 *Acta Crystallogr.* A **32** 751
Solntsev V P, Shcherbakova M Y and Dvornikov E V 1974 *J. Struct. Chem.* **15** 217
Speer J A 1980 Zircon *Orthosilicates (Rev. Mineral)* vol 5, ed P H Ribbe p 67
Thomas J B, Bodnar R J, Shimizu N and Sinha A K 2002 *Geochim. Cosmochim. Acta* **66** 2887
Tomkeleff S I 1946 *Sci. Prog.* **36** 696
Vance E R and Mackey D J 1974 *J. Phys. C: Solid State Phys.* **7** 1898
Vance E R and Mackey D J 1975 *J. Phys. C: Solid State Phys.* **8** 3439
Vance E R and Mackey D J 1978 *Phys. Rev.* B **18** 185
Watson E B 1980 *Geochim. Cosmochim. Acta* **44** 895
Weber W J, Ewing R C, Catlow C R A, de la Rubia T D, Hobbs L W, Kinoshita C, Matzke H, Motta A T, Nastasi M, Salje E H K, Vance E R and Zinkle S J 1998 *J. Mater. Res.* **13** 1434
Weber W J, Ewing R C and Lutze W 1996 *Mater. Res. Soc. Symp. Proc.* **412** 25
Williford R E, Begg B D, Weber W J and Hess N J 2000 *J. Nucl. Mater.* **278** 207
Woodhead J A, Rossman G R and Silver L T 1991a *Am. Mineral.* **76** 74
Woodhead J A, Rossman G R and Thomas A P 1991b *Am. Mineral.* **76** 1533
Zhang M, Lee G A, Salje E K H and Beran A 2001 *Am. Mineral.* **86** 904
Zhang M and Salje E K H 2001 *J. Phys.: Condens. Matter* **13** 3057
Zhang M and Salje E K H 2003 *Phase Transit.* **76** 117

Zhang M, Salje E K H, Capitani G C, Leroux H, Clark A M and Schlüter J 2000a *J. Phys.: Condens. Matter* **12** 3131
Zhang M, Salje E K H and Ewing R C 2002 *J. Phys.: Condens. Matter* **14** 3333
Zhang M, Salje E K H, Ewing R C, Farnan I, Ríos S, Schlüter J and Leggo P 2000b *J. Phys.: Condens. Matter* **12** 5189
Zhang M, Salje E K H, Farnan I, Graeme-Barber A, Daniel P, Ewing R C, Clark A M and Leroux H 2000c *J. Phys.: Condens. Matter* **12** 1915
Zhang M, Salje E K H, Malcherek T, Bismayer U and Groat L A 2000d *Can. Mineral.* **38** 119
Zhang M, Wruck B, Graeme-Barber A, Salje E K H and Carpenter M A 1996 *Am. Mineral.* **81** 92